SHORT COMMUNICATION

Oxidation processes on conducting carbon additives for lithium-ion batteries

Fabio La Mantia · Robert A. Huggins · Yi Cui

Abstract The oxidation processes at the interface between different types of typical carbon additives for lithium-ion batteries and carbonates electrolyte above 5 V versus Li/Li^+ were investigated. Depending on the nature and surface area of the carbon additive, the irreversible capacity during galvanostatic cycling between 2.75 and 5.25 V versus Li/Li^+ could be as high as 700 mAh g^{-1} (of carbon). In the potential region below 5 V versus Li/Li^+, high surface carbon additives also showed irreversible plateaus at about 4.1–4.2 and 4.6 V versus Li/Li^+. These plateaus disappeared after thermal treatments at or above 150 °C in inert gas. The influence of the irreversible capacity of carbon additives on the overall performances of positive electrodes was discussed.

Keywords Lithium-ion batteries · Conductive additives · High voltage positive electrode · Electrolyte stability window · Solid electrolyte interphase

1 Introduction

Lithium-ion batteries are now used in a wide range of applications, particularly in connection with portable electronic devices. The challenge of using these systems in larger applications such as for personal or public transportation requires improvements in energy and power density, and also cycle life. One of the major limitations to the improvement of the energy and power density in today's Li-ion batteries concerns the positive electrode material: the active materials used in most applications are the layer-structured $LiMO_2$ materials, with M = Co, Ni, Mn, or a mixture of them, or the olivine $LiFePO_4$. With the exception of overlithiated phases, all these compounds have very similar theoretical values of energy, if used with the same negative electrode (graphite or $Li_4Ti_5O_{12}$) [1–5].

Current efforts to increase the specific energy of Li-ion batteries are mainly focused on the investigation of lithiated compounds with high reaction potentials, above 4.6 V versus Li/Li^+ [6–10]. This is far beyond the stability window of the organic electrolytes [11, 12], which are then thermodynamically driven to be oxidized; stabilizing kinetically the active materials, for example through the formation of a more stable solid electrolyte interphase (SEI) [13, 14], becomes a challenge. Although the typical positive electrode contains a considerable volumetric amount of conductive carbon additives (such as Super-P, acetylene black, and graphite), the low percentage mass load (<8 wt%) of these compounds in the total electrode induces to consider such additives as inert or passive, which means they take a negligible part to the specific reversible and irreversible charge of the electrode. Graphite was also investigated as positive electrode, due to the possibility to intercalate anions from the electrolyte in its layered structure at high potentials (around 4.7 V vs. Li/Li^+ [15–17]), leading to a specific reversible charge of circa 140 mAh g^{-1}.

Considering the higher surface of the carbons additives in contact with the electrolyte, their relatively high conductivity and their higher affinity towards the carbonates, in this study we want to investigate the reversible and

F. La Mantia · R. A. Huggins · Y. Cui (✉)
Department of Materials Science and Engineering,
Stanford University, Stanford, CA 94305, USA
e-mail: yicui@stanford.edu

Present Address:
F. La Mantia
Zentrum für Elektrochemie, Ruhr-Universität Bochum,
Universitätsstr. 150, 44780 Bochum, Germany

irreversible-specific charge and the charge/discharge profiles for both low specific surface (graphite) and high specific surface (Super-P, acetylene black, and carbon nanofibers), in the attempt to understand their properties in the potential window between 2.75 and 5.25 V versus Li/Li$^+$, and their influence on the overall electrochemical performances of positive electrodes.

2 Experimental aspects

2.1 Scanning electron microscopy

SEM measurements were performed on a FEI XL30 Sirion microscope on uncoated powder samples. Images were recorded at 5 kV with a secondary electron beam.

2.2 BET measurements

Carbon powders weighing 150–250 mg were used to get the isotherms using Micromeritics porosity analyzer (ASAP 2020). Before actual adsorption measurements, the samples were degassed at 350 °C and high vacuum for ∼8 h. The BET area was obtained by analyzing the data in the range of $0.05 \leq P/P_0 \leq 0.3$.

2.3 Electrochemical measurements

Four different carbon additives were investigated: graphite (Fluka, product no. 78391); acetylene black (Alfa Aesar, product no. 45527); Super-P (TIMCAL); and carbon nanofibers (Aldrich, product no. 719781). The electrochemical cycling experiments were performed at room temperature in coffee-bag type cells with a two-electrode half-cell configuration, and metallic lithium serving as the counter electrode. The electrolyte was a 1 M solution of LiPF$_6$ in a 1:1 by weight mixture of EC and DMC (Ferro). Galvanostatic cycling was performed with a Versatile Multichannel Potentiostat, VMP3 (Bio-Logic SA) between the cut-off potentials of 2.75 and 5.25 V versus Li/Li$^+$. No potentiostatic step was applied.

Pure carbon working electrodes were prepared using the "doctor-blading" technique, starting from an *N*-methyl pyrrolidone (NMP) (Aldrich, product no. 328634) based slurry with the carbon powders and polyvinylidene fluoride (PVdF) as binder (Fluka, $M_W = 530,000$). The weight percent of the carbon powders depended on the type of carbon: 80 % for graphite-based electrodes, and 40 % for the other carbon powder-based electrodes. The slurry was doctor bladed onto aluminum current collectors and then dried at 90 °C in air overnight. The samples were transferred in a glove box with a high purity argon atmosphere (O$_2$ < 1 ppm, H$_2$O < 1 ppm). The thermally treated samples were heated on a hot plate at 100, 150, or 200 °C inside the glove box for 3 h. All the pure carbon working electrodes were cycled at a specific current of 20 mA g^{-1}.

Alumina–carbon working electrodes were also prepared using the doctor-blading technique, starting from an NMP-based slurry with Al$_2$O$_3$ (J.T. Baker Chemical Co.) (81 wt%), Super-P (TIMCAL) (9 wt%), and polymeric binder (PVdF) (10 wt%). These electrodes were used to simulate the performances of a real composite electrode, with Al$_2$O$_3$ keeping the carbon particles apart, as the active material would do. Being Al$_2$O$_3$ inert, these electrodes allowed the study of the carbon additives in a real geometry. These samples were also transferred into the glove box and thermally treated on a hot plate at 150 °C for 3 h. The alumina–carbon working electrodes were cycled at specific currents of 150 and 100 mA g^{-1} of Super-P, simulating 16.7 and 11.1 mA g^{-1} of Al$_2$O$_3$ specific currents, respectively.

3 Results and discussion

SEM pictures of the carbon-containing samples are shown in Fig. 1. Acetylene black and Super-P (Fig. 1a, c) powders are very similar; both of them are composed of micrometric aggregates of sub-micrometric particles. The carbon nanofibers powder (Fig. 1b) has a fiber structure, as expected, with some round-shaped particles. Graphite powder (Fig. 1d) is composed only of micrometric particles with large flake-like shape.

In Table 1, the measured BET area of the different carbon additives is reported. The highest BET surface is observed for acetylene black and Super-P, followed by the carbon nanofibers. As expected, graphite particles have the lowest surface area.

Pure carbon working electrodes were tested in the high potential region, above 5 V versus Li/Li$^+$, to investigate their properties under a highly oxidative environment. The charge/discharge profile of the carbon additive is important for understanding the irreversible processes due to side reactions occurring on its surface. The most probable side reaction in this potential range is the oxidation of the electrolyte, and formation of a SEI. The latter occurs upon both the active material and the carbon additive. The very first cycles were investigated in this study, for that is when the irreversible capacity is normally higher.

Figure 2a shows the charge/discharge profiles of different carbon additives during the first cycle in the standard electrolyte at 20 mA g^{-1}. The test cell was assembled immediately after transferring the hot electrodes (90 °C) into the glove box, without further heat treatment. It is observed that the irreversible capacity is strongly dependent on the type of carbon additive. In particular, acetylene
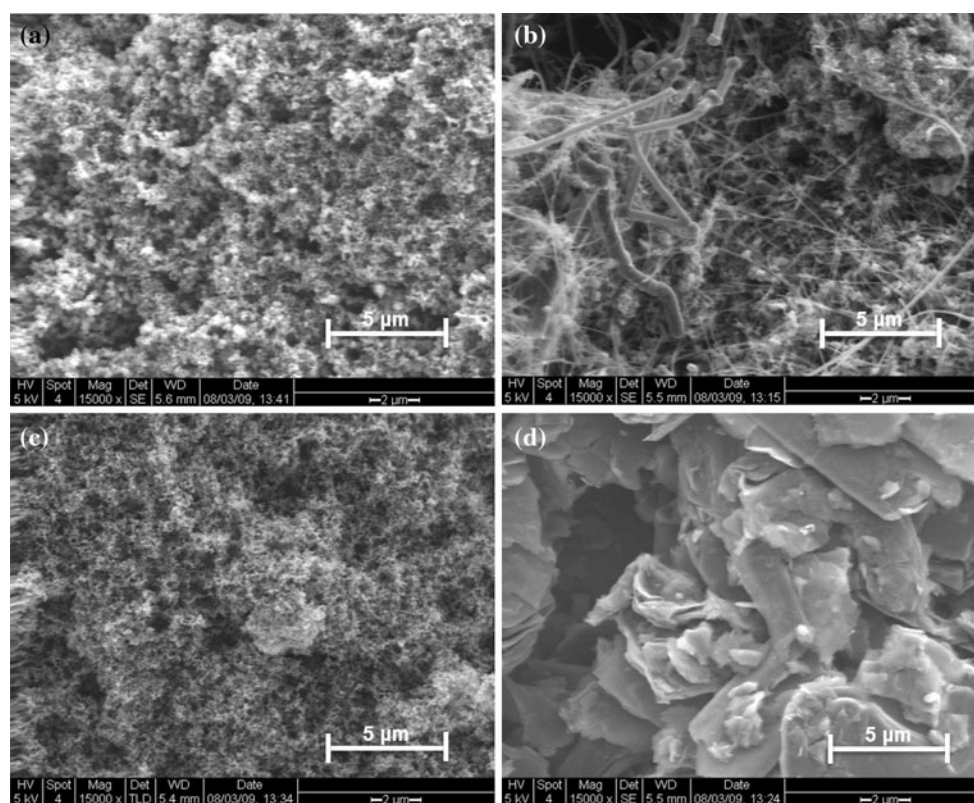
Fig. 1 SEM pictures of the carbon powders. **a** acetylene *black*; **b** carbon nanofibers; **c** Super-P; **d** graphite

black has the highest irreversible capacity (above 700 mAh g^{-1}), followed by the carbon nanofibers, Super-P, and graphite. Acetylene black, Super-P, and carbon nanofibers have a linear discharge profile, which is clear proof of double layer discharging. On the other hand, the graphite shows a plateau around 4.5 V versus Li/Li$^+$. This plateau is due to the deintercalation of PF$_6$$^-$, a known process. The specific reversible charge reported in this study is much less than that previously reported [16], because of the chosen potential limits. The type of graphite influences the reversible specific charge, as well. In Fig. 2b, a zoom-in version of Fig. 2a for small Q is shown. Some peaks and plateaus are observed for the high surface carbon additives in the potential region 4.1–4.2 V versus Li/Li$^+$. This behavior is observed in acetylene black, Super-P, and carbon nanofibers; it is quite random, both in the position and in the length of the plateaus, and influences only slightly the total performance of the electrode. Another plateau is observed around 4.6 V versus Li/Li$^+$ in the experiments on acetylene black and Super-P. This is longer than the former and always appears at the same potential, with a length that is quite constant from sample to sample and significantly influences the performance of the electrode, in terms of specific irreversible charge.

In Table 1, the specific irreversible charge and the density of irreversible charge (with respect to the BET

Table 1 Characteristics and irreversible charge for the different carbon additives investigated. Q_{irr} and q_{irr} are the specific irreversible charge and the density of irreversible charge with respect to the BET area, respectively

Type	BET (m^2 g^{-1})	Q_{irr} (mAh g^{-1})	q_{irr} (mC cm^{-2})
Black acetylene	64	737	4.15
Carbon Nanofibers	36	624	6.24
Super-P	65	484	2.68
Graphite	13	143	3.96

area) are reported for the different carbon additives. We want to stress that the differences in the density of irreversible charge, being not correlated to geometrical effects, are due to the nature of the carbon additives. These differences could be caused by the nature of the surface groups, which depend on the synthesis condition of the carbon additive. The best result is obtained with Super-P, while acetylene black and graphite have similar density of irreversible charge.

Due to the low specific irreversible charge and charge density, Super-P electrodes were selected for further investigation. The charge/discharge profile of Super-P electrodes during the first cycle in the standard electrolyte at 20 mA g^{-1} is reported in Fig. 3a. The samples were
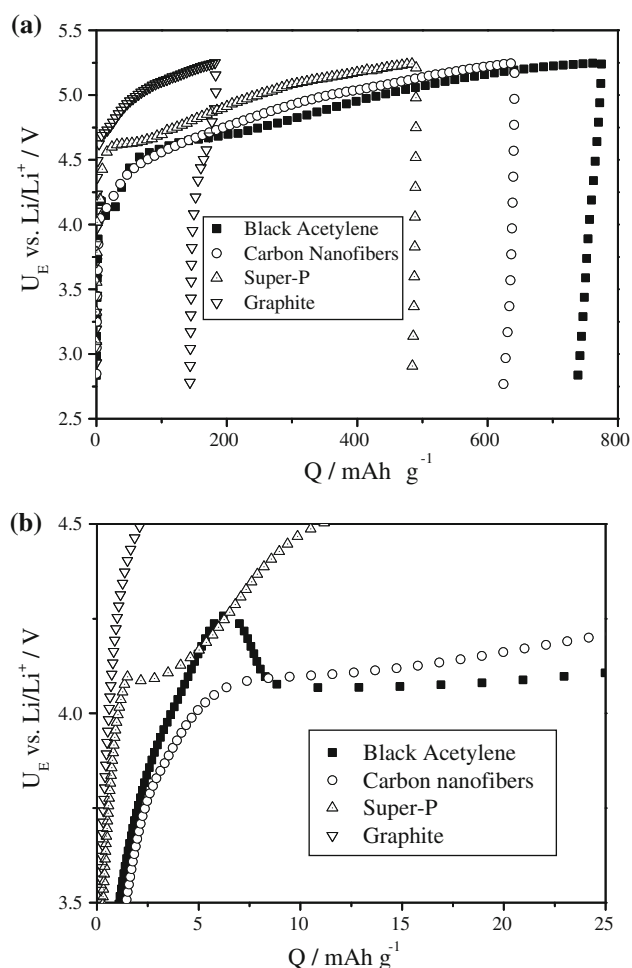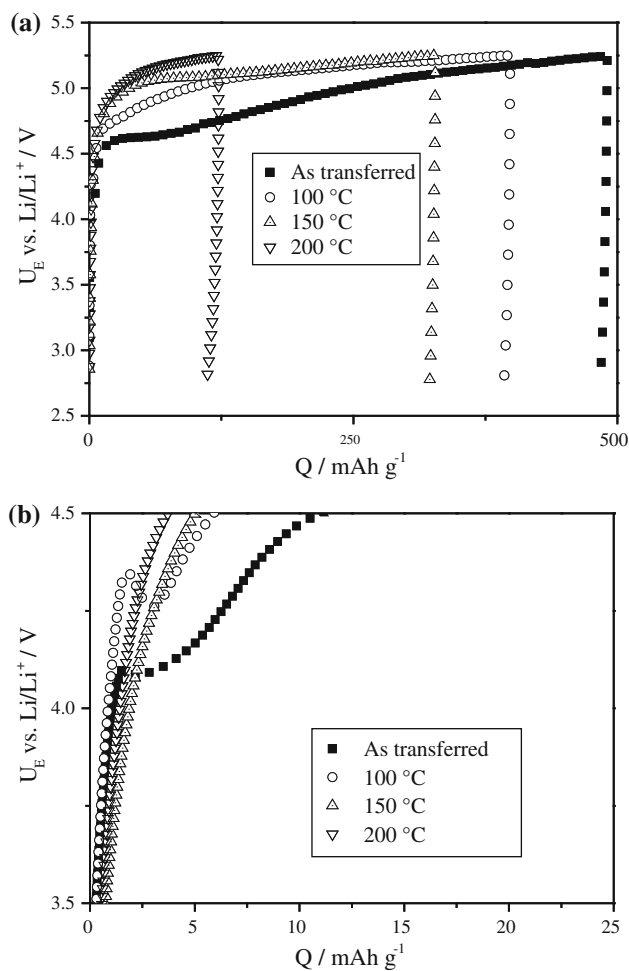
Fig. 2 Charge/discharge profile of the investigated carbon additives during the first cycle in the potential window 2.75–5.25 V versus Li/Li$^+$ in the 1 M LiPF$_6$, EC:DMC (1:1 wt) electrolyte. The electrodes were backed only at 90 °C in the air, and the cells were assembled immediately after the transfer in the glove box

heated up after transfer in the glove box at 100, 150, and 200 °C, respectively, to test the effect of volatile impurities on their performance. As a general trend, it was observed that the specific irreversible charge decreased by increasing the temperature of the thermal treatment. In particular, the low voltage plateau, at 4.1–4.2 V versus Li/Li$^+$ disappeared for all the baking temperatures at or above 100 °C (see Fig. 3b). The length of the higher voltage plateau depended strongly on the temperature of the thermal treatment. We believe that the first plateau, at 4.1 V versus Li/Li$^+$, is due to adsorbed water, while the second plateau, at 4.6 V versus Li/Li$^+$, is generated by the oxidation of surface groups or the oxidation of the electrolyte, and consequent formation of a SEI-like layer. To support this theory, it is noted that the standard oxidation potential of water should be around 4.25 V versus Li/Li$^+$. We want to emphasize also that the main difference in the charge/discharge profiles of the sample treated at 150 °C and the one

treated at 200 °C is above 5 V versus Li/Li$^+$, while the samples treated at 100 °C showed differences (with respect to the sample treated at 200 °C) already at a lower potential, about 4.5 V versus Li/Li$^+$.
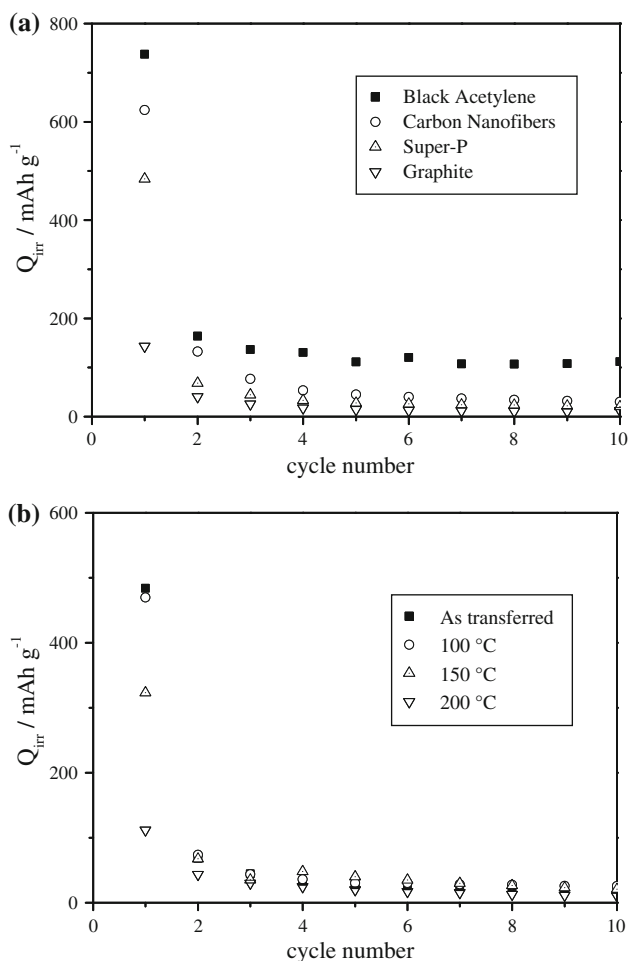
The irreversible-specific charge, Q_{irr}, of the different carbons additives and the different thermal treatment (only for Super-P) versus cycle number is reported in Fig. 4. It can be observed that Q_{irr} decreases strongly upon cycling, but it is never reduced to 0. The thermal treatment seems to affect primarily the first cycle, but not the following ones. Indeed, in the charge/discharge profile (not shown here) of later cycles, all the features relative to adsorbed water and other impurities disappear, the same as was found after the thermal treatment. The irreversible-specific charge of the Super-P treated at 200 °C is much smaller than the others at all cycles. This is an effect of a reduced specific charge during charging and an enhanced specific charge during the discharge. The reason of this dramatic change is not clear;

Fig. 3 Charge/discharge profile of Super-P, heated up in glove box for 3 h at different temperatures, during the first cycle in the potential window 2.75–5.25 V versus Li/Li$^+$ in the 1 M LiPF$_6$, EC:DMC (1:1 wt) electrolyte

nevertheless we would like to suggest one hypothesis. It is possible that, when the sample is heated at 200 °C, the melted PVdF (T_m = 171 °C) covers in a more complete way the carbon particles, protecting them from the liquid electrolyte. It has been observed that the SEI is not formed on the PVdF binder [18, 19], which would justify the tremendous decrease in Q_{irr} for the treatment at 200 °C. Further investigations are going to be carried out and will be the aim of future work.
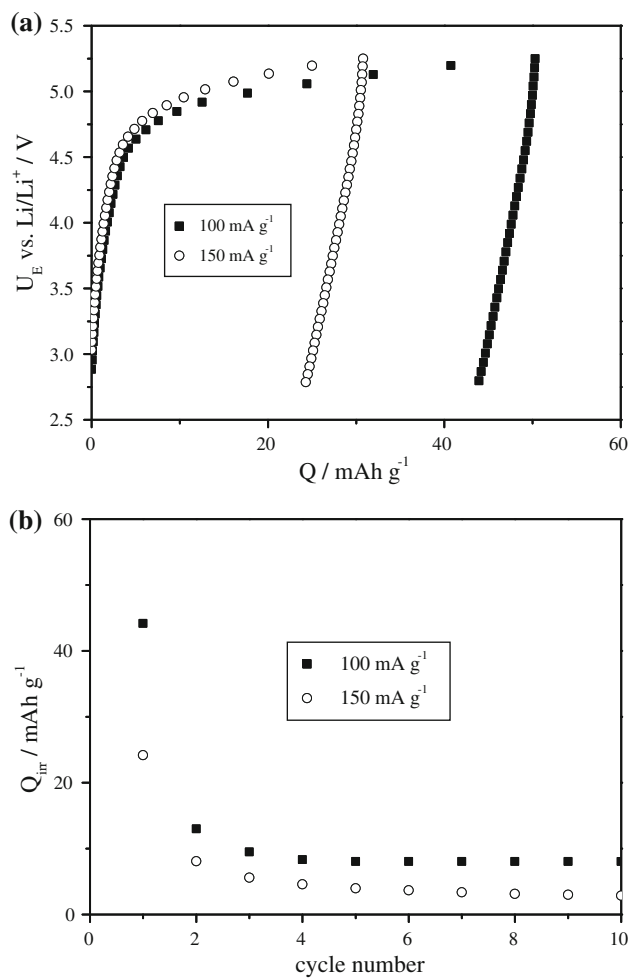
To test the effect of a more realistic geometry (the presence of active material) and more realistic current rates (the weight of the carbons is normally much smaller than the weight of the active material) a set of electrodes was made by mixing together Super-P and alumina particles. The ratio between Super-P and alumina was similar to that used in real laboratory electrodes. In Fig. 5, the charge/discharge profile of the first cycle and the irreversible charge versus cycle number in the standard electrolyte at different current rates (100 and 150 mA g^{-1} of Super-P) are

reported. The samples were heated up to 150 °C for 3 h after transfer in the glove box to remove traces of water and other impurities. A direct comparison between the different current rates and the results reported in Figs. 3 and 4 for the Super-P cycles at 20 mA g^{-1} after the thermal treatment at 150 °C reveals that the current rate has a very strong effect on the specific irreversible charge of the conductive carbon additives; the higher the current rate, the lower the specific irreversible charge. This is realistically related to the time that the electrode spends at high potential.

The strong dependence of the specific irreversible charge on the current rate and on the cycle number suggests the formation of a SEI-like protective layer on the surface of the carbon additive, probably composed of the products of oxidation of the electrolyte. This SEI-like layer strongly reduces the oxidation rate after the first cycle, but does not block it completely. If the cycling is interrupted for 1 day and then started again (not shown here), the value of the

Fig. 4 Irreversible-specific charge versus cycle number. **a** Carbon additives, cell assembled immediately after the transfer in the glow box. **b** Super-P after different thermal treatments for 3 h in glove box

Fig. 5 a Charge/discharge profile and (**b**) irreversible-specific charge versus cycle number at different current rates of Al_2O_3/Super-P electrodes, heated up in glove box for 3 h at 150 °C, during the first cycle in the potential window 2.75–5.25 V versus Li/Li$^+$ in the 1 M LiPF$_6$, EC:DMC (1:1 wt) electrolyte

specific irreversible charge is similar to the one of the second and later cycles, suggesting that this SEI-like layer is effectively stable, or at least has a stable component. The SEI layer formed on the surface of common active materials for positive electrodes was investigated by many authors [14, 20, 21]. We believe that the similar compounds produced by the oxidation of the electrolyte, such as Li_2CO_3, LiF, and polycarbonates, should be present on the SEI layer of the carbon additives. It is noteworthy to stress that, for the carbon additives, it is not necessary that the SEI layer is ionically conductive.

Even if the high current rate results show that the specific irreversible charge can be very low, relative to the reversible charge of a possible active material, the conditions under which the carbon additive interacts with the electrolyte strongly depends on the active material itself. Indeed, the longer the charge/discharge plateau of the active material and the higher its potential, the more time the carbon additive will spend in the high potential region. As consequence, the specific irreversible charge will increase. To properly evaluate experiments on real electrodes, containing both an active material and a carbon additive, one needs to know the detailed electrochemical behavior of the carbon additive, and subtract it from the observed results.

4 Conclusions

Experiments on different types of carbon additives have shown that they can be a significant source of specific irreversible charge, in some cases higher than 700 mAh g^{-1}. The value of the irreversible-specific charge is dependent on the nature of the carbon additive and thermal treatments. There is generally a strong reduction of the specific irreversible charge after the first cycle. Experiments at different current rates have suggested that the main mechanism occurring during the charge of the carbon additives is the formation of a SEI-like layer, probably composed of products of the oxidation of the electrolyte. However, further post-mortem investigations are necessary to confirm this explanation and will be the aim of future work.

References

1. Tarascon JM, Wang E, Shokoohi FK, McKinnon WR, Colson S (1991) The spinel phase of $LiMn_2O_4$ as a cathode in secondary lithium cells. J Electrochem Soc 138(10):2859–2864. doi:10.1149/1.2085330

2. Ohzuku T, Makimura Y (2001) Layered lithium insertion material of $LiCo_{1/3}Ni_{1/3}Mn_{1/3}O_2$ for lithium-ion batteries. Chem Lett 30(7):642–643. doi:10.1246/cl.2001.642

3. Whittingham MS (2004) Lithium batteries and cathode materials. Chem Rev 104(10):4271–4301. doi:10.1021/cr020731c

4. Takahashi M, Tobishima S, Takei K, Sakurai Y (2002) Reaction behavior of $LiFePO_4$ as a cathode material for rechargeable lithium batteries. Solid State Ionics 148(3–4):283–289. doi:10.1016/S0167-2738(02)00064-4

5. Liu HW, Tang DG (2008) The low cost synthesis of nanoparticles $LiFePO_4$/C composite for lithium rechargeable batteries. Solid State Ionics 179(33–34):1897–1901. doi:10.1016/j.ssi.2008.05.005

6. Ruffo R, Huggins RA, Mari CM, Piana M, Weppner W (2005) Phosphate materials for cathodes in lithium ion secondary batteries. Ionics 11(3–4):213–219. doi:10.1007/BF02430379

7. Pasero D, Reeves N, Pralong V, West AR (2008) Oxygen non-stoichiometry and phase transitions in $LiMn_{1.5}Ni_{0.5}O_{4-\delta}$. J Electrochem Soc 155(4):A282–A291. doi:10.1149/1.2832650

8. Ma J, Qin QZ (2005) Electrochemical performance of nanocrystalline $LiMPO_4$ thin films prepared by electrostatic spray deposition. J Power Sources 148:66–71. doi:10.1016/j.jpowsour.2005.01.041

9. Lloris JM, Vicente CP, Tirado JL (2002) Improvement of the electrochemical performance of $LiCoPO_4$ 5 V material using a novel synthesis procedure. Electrochem Solid State Lett 5(10):A234–A237. doi:10.1149/1.1507941

10. Wolfenstine J, Allen J (2005) Ni^{3+}/Ni^{2+} redox potential in $LiNiPO_4$. J Power Sources 142(1–2):389–390. doi:10.1016/j.jpowsour.2004.11.024

11. Holzapfel M, Wursig A, Scheifele W, Vetter J, Novák P (2007) Oxygen, hydrogen, ethylene and CO_2 development in lithium-ion batteries. J Power Sources 174(2):1156–1160. doi:10.1016/j.jpowsour.2007.06.182

12. Xu K (2004) Nonaqueous liquid electrolytes for lithium-based rechargeable batteries. Chem Rev 104(10):4303–4417. doi:10.1021/cr030203g

13. La Mantia F, Rosciano F, Tran N, Novák P (2009) Quantification of oxygen loss from $Li_{1+x}(Ni_{1/3}Mn_{1/3}Co_{1/3})_{1-x}O_2$ at high potentials by differential electrochemical mass spectrometry. J Electrochem Soc 156(11):A823–A827. doi:10.1149/1.3205495

14. Aurbach D, Gamolsky K, Markovsky B, Salitra G, Gofer Y, Heider U, Oesten R, Schmidt M (2000) The study of surface phenomena related to electrochemical lithium intercalation into Li_xMO_y host materials (M = Ni, Mn). J Electrochem Soc 147(4):1322–1331. doi:10.1149/1.1393357

15. Jobert A, Touzain P, Bonnetain L (1981) Intercalation of PF6-, AsF6- and SbF6-ions into graphite by an electrochemical method—characterization of the products obtained. Carbon 19(3):193–198. doi:10.1016/0008-6223(81)90042-7

16. Seel JA, Dahn JR (2000) Electrochemical intercalation of PF_6 into graphite. J Electrochem Soc 147(3):892–898. doi:10.1149/1.1393288

17. Ishihara T, Koga M, Matsumoto H, Yoshio M (2007) Electrochemical intercalation of hexafluorophosphate anion into various carbons for cathode of dual-carbon rechargeable battery. Electrochem Solid State Lett 10(3):A74–A76. doi:10.1149/1.2424263

18. Yamaki J, Takatsuji H, Kawamura T, Egashira M (2002) Thermal stability of graphite anode with electrolyte in lithium-ion cells. Solid State Ionics 148(3–4):241–245. doi:10.1016/s0167-2738(02)00060-7

19. Dedryvere R, Martinez H, Leroy S, Lemordant D, Bonhomme F, Biensan P, Gonbeau D (2007) Surface film formation on electrodes in a $LiCoO_2$/graphite cell: a step by step XPS study. J Power Sources 174(2):462–468. doi:10.1016/j.jpowsour.2007.06.033

20. Veluchamy A, Doh CH, Kim DH, Lee JH, Shin HM, Jin BS, Kim HS, Moon SI (2009) Thermal analysis of Li_xCoO_2 cathode material of lithium ion battery. J Power Sources 189(1):855–858. doi:10.1016/j.jpowsour.2008.07.090

21. Edstrom K, Gustafsson T, Thomas JO (2004) The cathode–electrolyte interface in the Li-ion battery. Electrochim Acta 50(2–3):397–403. doi:10.1016/j.electacta.2004.03.049